



Dynamic and Static Analysis of LNG Tank Dome Mesh Shell Structure

Jiedong Zhan^a, Chenguang Liang*, Jichong Zhao^b

Northeast Petroleum University, Daqing 163318, China

^azjd700617@sina.com, ^{*}996292142@qq.com, ^b937471617@qq.com

Abstract. The rib-and-ring single-layer spherical mesh shell structure is widely used in the mesh shell structure of LNG tank domes because of its simple installation, convenient construction and excellent mechanical properties. In order to study the mechanical properties of the mesh-shell structure of the tank, the overall model of the 30,000 m³ LNG full-capacity tank was established by using ANSYS software, and static analyses were carried out based on three different combinations of working conditions, and the structural strength and stiffness met the requirements of the specification. Subsequently, the eigenvalue buckling analysis of the mesh shell structure and the effect of initial geometric defects on the stability of the mesh shell structure are analyzed in depth, and finally, the effects of different seismic waves on the structure under one-dimensional seismic action are investigated, and the results show that: when the magnitude of the initial geometric defects increases, the ultimate load carrying capacity of the mesh shell decreases significantly, and when the magnitude of the initial geometric defects is less than 1/700, there is no significant difference in the ultimate load carrying capacity with the perfect structure. It is suggested to take the initial geometric defect amplitude lower than 1/700 of the structural amplitude of the mesh shell. In one-dimensional seismic analysis, the effects of different seismic waves on the structural displacements and peak axial forces of the rods are large, so it is necessary to combine a variety of seismic waves, and the strength of the local mesh shell rods needs to be improved.

Keywords: LNG storage tank; ribbed annular spherical mesh shell; static analysis; initial geometric defects; dynamic analysis

1 Instructions

The LNG dome mesh shell mostly adopts rib-ring type single-layer spherical mesh shell structure [1,2], which is a kind of spatial rod system structure similar to the flat plate mesh frame, and a spatial frame composed of mesh based on rods according to a certain law and arranged according to the shell structure. The structure has the properties of both the rod system and the shell, and its force transmission is mainly characterized by point-by-point force transmission through the tension, pressure or shear force in two

directions within the shell. Single-layer mesh shell structure needs to meet certain stiffness and strength requirements.

There are many types of steel mesh shell structure, once the design is not selected properly, it is very easy to cause the mesh shell structure instability, triggering engineering accidents. 1963, located in Galester, Romania, a single-storey mesh shell structure with a span of 93.5m in the role of the snow load occurred in the overall destabilization of the structure and then triggered a structural collapse of the accident, so that people pay more attention to the mesh shell structural stability problems. In the 1930s, Donnell proposed that the post-buckling state of thin-shell should be calculated by nonlinear large deflection theory to determine the critical load of the structure. 1939, China's famous scholars Qian Xuesen and Karman [3] carried out a nonlinear analysis of the thin-shell structure, which came to the conclusion that the difference between the actual bearing capacity and the structure is not large, and put forward the nonlinear theory of the structure. Their viewpoints provide a solid theoretical basis for subsequent nonlinear analysis of thin-shell structures[4,5]. Initial geometric defects refer to the phenomena such as displacement deviation of mesh-shell nodes, eccentricity of mesh-shell rods, or bending of rods during processing, which greatly weaken the stability of mesh-shell structures and have a significant impact on the stability of the structure, and thus become one of the unavoidable problems in the study of mesh-shell structures [6,7].

2 Finite Element Modeling Approach Validation and Model Building

2.1 Validation of Structural Modeling Methods for Mesh Shells

The single-layer mesh shell structure used in Ye Jihong's experiment in the literature [9] has a sagittal height of 0.13 m, a span of 2.5 m, and consists of 24 rods with a steel tube cross-section of 19.3 mm*1.4 mm, as shown in Fig. 1. The weight of the apex in the experiment is 46.2 kg, and the peripheral nodes are weighted with 20 kg. The model is modeled using the steel structure design software 3D3S and imported into ANSYS for modal analysis, and the first six orders of intrinsic frequencies are calculated by Lanczos method as shown in Table 1 and compared with Table 2. The Lanczos method was used to calculate the self-oscillation characteristics. The first six orders of the intrinsic frequency are shown in Table 1, and the comparison between the finite element model and the literature is shown in Table 2.

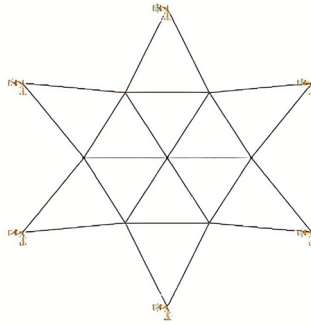


Fig. 1. Single-layer mesh shell model used in Ye Jihong's experiments

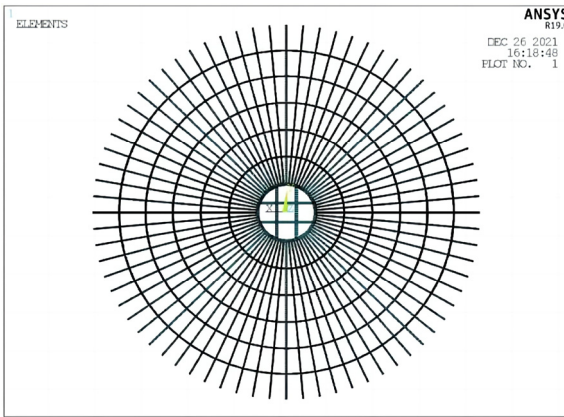


Fig. 2. Model drawing of single-layer ribbed ring reticulated shell structure

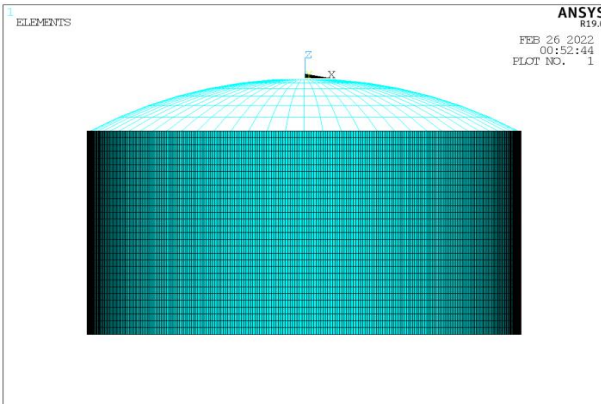


Fig. 3. Overall simplified model of LNG storage tank

Table 1. The first six orders of intrinsic frequency of the finite element model

Number of fixed-frequency steps	1	2	3	4	5	6
Finite element model intrinsic frequency	6.830	9.980	9.980	10.793	10.793	12.081
Measured values from tests in the literature	6.346	10.724	-	-	-	-
Relative error	7.62%	6.93%	-	-	-	-

Finite element simulation results and literature measured values are in good agreement, the first order error of both is 7.62%, and the second order error is 6.93%, which meets the requirements of engineering calculations. It can be seen that the mesh shell structure established by this modeling method is reasonable.

2.2 Finite Element Modelling of Storage Tanks

In this paper, according to a 30,000 LNG full capacity tank, the lower layer of the dome is a single-layer rib-ring type steel mesh shell, and the mesh shell structure is welded to the pressure ring of the tank wall; the LNG dome tank is a rib-ring type single-layer mesh shell structure, with a total of seven rings, and radial beams spaced at 10° in each ring, with a total of 72 radial H-type beams; the center ring structure is set up as four Tic-Tac-Logic beams, with the center ring beams, the center ring Tic-Tac-Logic beams, and the inner 2 rings of ring The center ring beam, center ring tic-tac-toe steel beam and inner 2 ring beams are H-type steel beam structures; the 3rd-6th ring beam structures are L-type steel beams. The dimensions of the steel beams are shown in Table 2, and steel beam material parameters shown in Table 3. Single layer mesh shell model is shown in Fig. 2, and the overall tank model is shown in Fig. 3

Table 2. Section size of steel beam

Steel Beam Type	Steel section form	Section size
Center Ring Ring Beam	H-beam	HW300×300×10×15
Center Tic-Tac-Toe Beam	H-beam	HW300×300×10×15
Radial beam	H-beam	HW175×175×7.5×7.5
2nd ring ring girder	H-beam	HW175×175×7.5×7.5
3rd-6th ring girders	Inverted L-beam	L160×160×12

Table 3. Material parameter

Steel Beam Material	Elastic Modulus (N/m ²)	Yield Strength (N/mm ²)	Density (kg/m ³)	Poisson Ratio
EN10025 S355 J12	2.0×10^5	345	7850	0.3

2.3 Load Values and Working Condition Combinations

According to the relevant norms and literature, the constant load + design internal pressure has a greater impact on the mesh shell structure. The corresponding load combination condition is "fixed constant load + live load + design vacuum pressure". 48.7m span mesh shell structure, self-weight is about 0.5, mesh shell Meng 5mm thick steel plate converted to surface load is about 0.5, and structural self-weight (constant load) is 1.0, the design value of the live load is 0.5, and the design of the internal pressure is 0.5; When calculating, the design internal pressure is included in the live load and the live load is 0.75. Due to the large influence of temperature conditions on the mesh shell structure, this paper will consider the temperature load T1=25°C and temperature load T2=-10°C during the construction of the LNG mesh shell structure.

The combinations of static calculation conditions for tank domes are mainly:

Condition 1: 1.2 constant load + 1.4 live load;

Condition 2: 1.2 constant load + 1.4 live load + 1.4 warming temperature load;

Condition 3: 1.2 constant load + 1.4 live load + 1.4 cooling temperature loads.

3 Structural Stiffness and Strength Analysis of LNG Dome Grid Shell Structures

3.1 Structural Rigidity Analysis of the Dome Mesh Shell of LNG Storage Tanks

According to GB50341-2014 "Design Code for Vertical Cylindrical Steel Welded Oil Tanks", the maximum displacement of the mesh shell can not exceed 1/400 of the diameter of the tank, and the diameter of the LNG storage tank is 48.7m, which means that the maximum displacement of the dome mesh shell structure can not exceed 122mm.

Under the three working conditions, ANSYS is used for static analysis of the overall model of the tank, and the results of the displacement analysis under the static force of the single-layer mesh shell are shown in Fig. 4, Fig. 5 and Fig. 6. The results of the mesh shell displacements under the three operating conditions are shown in Table 4.

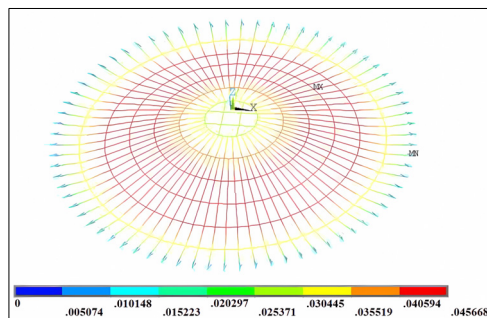


Fig. 4. Cloud image of overall displacement of single-layer reticulated shell storage tank under working condition 1

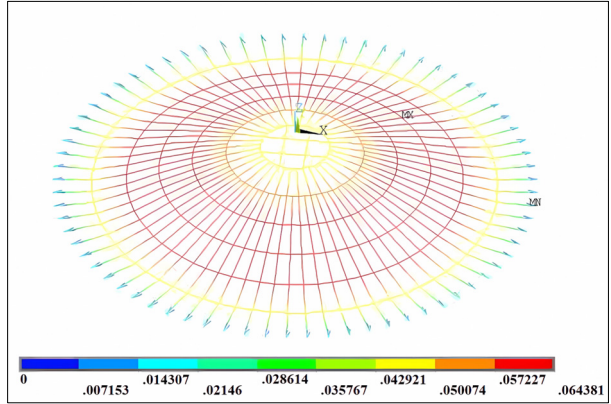


Fig. 5. Cloud image of overall displacement of single-layer reticulated shell storage tank under working condition 2

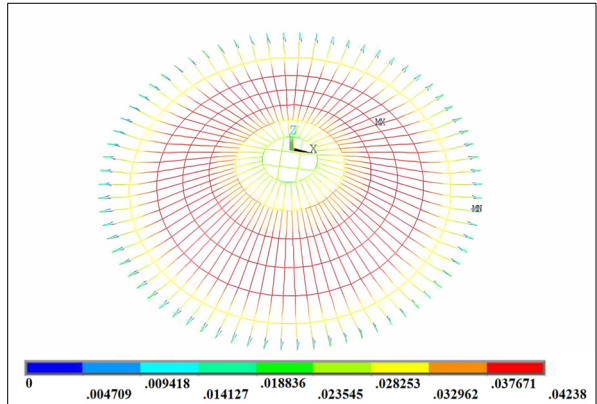


Fig. 6. Cloud image of overall displacement of single-layer reticulated shell storage tank under working condition 3

Table 4. Displacement results of reticulated shell under three working conditions

Model	Displacement(mm)	Maximum displacement node
Condition 1	45.7	240
Condition 2	64.3	238
Condition 3	42.38	148

The overall model of the tank under working condition 1 shows the maximum displacement at node 240, with a displacement value of 45.7 mm, and the maximum displacement at node 64.3 mm under working condition 2, and the maximum displacement at node 148 under working condition 3, with a maximum value of 30.94. The maximum values of the model displacements for the three conditions are less than 122 mm, which meet the requirements of the mesh and shell structural rigidity.

3.2 Strength Analysis of LNG Tank Dome Mesh Shell Structure

The strength of a mesh shell member that is a tension member or compression member subject to bending moments in the plane shall satisfy formula (1).

$$\frac{N}{A_n} \pm \frac{M_x}{\gamma_x W_{nx}} \pm \frac{M_y}{\gamma_y W_{ny}} \leq f \tag{1}$$

Where N =the axial tension or axial pressure (N); A_n =the net cross-sectional area (mm^2); M_x =the bending moment of the cross-section around the X-axis ($\text{N}\cdot\text{mm}$); γ_x =the coefficient of plastic development of the cross-section, for the I-section = 1.05; W_{nx} =the net sectional modulus to the x-axis (mm^3); M_y =the bending moment of the section about the y-axis ($\text{N}\cdot\text{mm}$); γ_y =the coefficient of plastic development of the section, for I-section $\gamma_y = 1.20$; W_{ny} =the net sectional modulus to the y-axis (mm^3); f =the design value of tensile, compressive and flexural strength (MPa), and the value of Q345-B in the Code for the Design of Steel Structures 310MPa.

The location of the pump well on the mesh shell structure is the part with the largest local load, and it is necessary to calculate the internal force of the mesh shell rods here, and its bending strength should satisfy formula (2).

$$\frac{M_x}{\gamma_x W_{nx}} \pm \frac{M_y}{\gamma_y W_{ny}} \leq f \tag{2}$$

The shear strength shall satisfy formula (3).

$$\tau = \frac{VS}{It_w} \leq f_v \tag{3}$$

Where τ =the shear stress (MPa); V =the shear force acting along the plane of the web in the calculated section (N); S =the area moment of the gross section centering and axis above the calculated shear stress (mm^3); I =the moment of inertia of the gross section (mm^4); t_w =the web thickness (mm); f_v =the strength design value (MPa), and the value of Q345-B in the Code for Design of Steel Structures is 180Mpa.

The calculated maximum stresses of this model rod are analyzed under three working conditions as shown in Fig. 7, Fig. 8 and Fig. 9. The results of the stresses in the mesh shell under the three operating conditions are shown in Table 5.

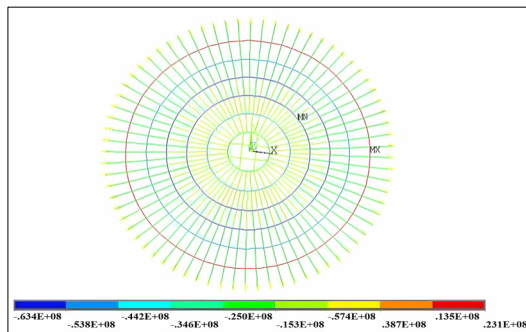


Fig. 7. Mises stress nephogram of overall tank model under 1 working condition

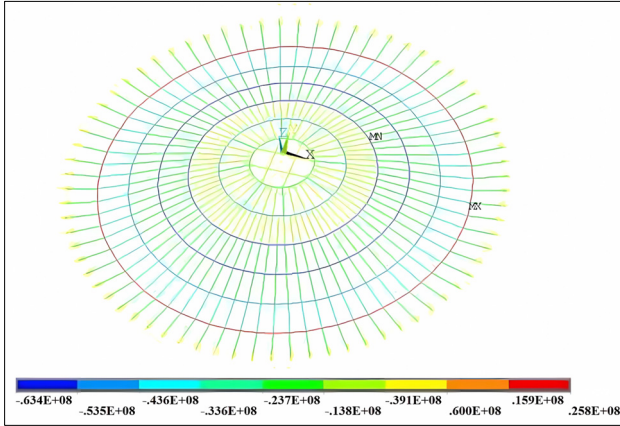


Fig. 8. Mises stress nephogram of overall tank model under 2 working condition

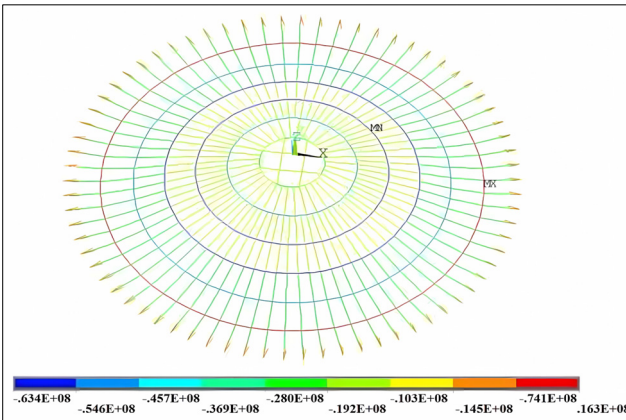


Fig. 9. Mises stress nephogram of overall tank model under 3 working condition

Table 5. Stress results of reticulated shell under three working conditions

Model	Maximum compressive stress (MPa)	Maximum compressive stress unit
Condition 1	63.4	280
Condition 2	63.4	261
Condition 3	63.4	261

The stress of any part of the mesh shell structure can not be greater than the stress of the corresponding material, and the permissible stress of the material Q345 steel is taken as $345/1.6=216\text{MPa}$, i.e., the maximum stress value of the rod can not exceed 216MPa .

The analysis shows that: the model under working condition 1, the maximum compressive stress occurs in unit 280, and the value of compressive stress is 63.4MPa . The maximum pressure unit occurs in the third ring, which indicates that the lower support

structure has less influence on the stress of the mesh shell. The maximum tensile stress under the action of Case 2 is 63.4 MPa, and the maximum tensile stress cell is cell 261 in the 2nd ring. The maximum compressive stress under condition 3 is 63.4 MPa, which occurs at unit 261 of ring 3. The maximum stress value of the structure under the three conditions is less than the permissible stress value of Q345 material, which meets the structural strength requirements of the mesh shell.

4 Stability Analysis of LNG Dome Mesh Shell Structure

4.1 Eigenvalue Buckling Analysis of LNG Single-Layer Spherical Mesh Shell Structure

The LNG tank mesh shell structure, the tank mesh shell nodes are designed with rigid joint nodes, the nodes account for 20% of the mesh shell weight when considering the mesh shell self-weight, and the bottom nodes are designed with solid joints. All the nodes are constrained to be solved at one time, and the support reaction force of the nodes is extracted, and Mass21 is used to convert the support reaction force into mass units. After calculation, the first 20 orders of buckling coefficients of the steel mesh shell structure are shown in Table 6.

Table 6. Stress results of reticulated shell under three working conditions

Order	Buckling coefficient	Order	Buckling coefficient
1	5.56	11	8.70
2	5.56	12	9.99
3	6.78	13	10.00
4	6.81	14	10.00
5	7.04	15	10.24
6	7.39	16	10.55
7	7.53	17	10.61
8	8.48	18	10.61
9	8.48	19	10.85
10	8.69	20	10.85

The first 6 orders of buckling modes of the tank mesh shell structure are shown in Fig. 10-15. From the eigenvalue buckling analysis of the LNG dome mesh shell structure, it can be seen that since the mass and stiffness of the LNG mesh shell structure are symmetrically distributed, the eigenvalue buckling deformation of the mesh shell presents left-right deformation predominantly at the first 2 orders, and the structural deformation at the 4-6 orders presents overall deformation. The adjacent two orders of eigenvalue buckling deformation show symmetric distribution, and the adjacent two orders of buckling eigenvalues are also similar.

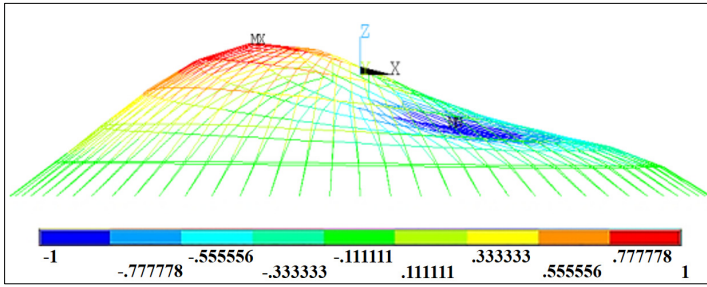


Fig. 10. First order buckling mode

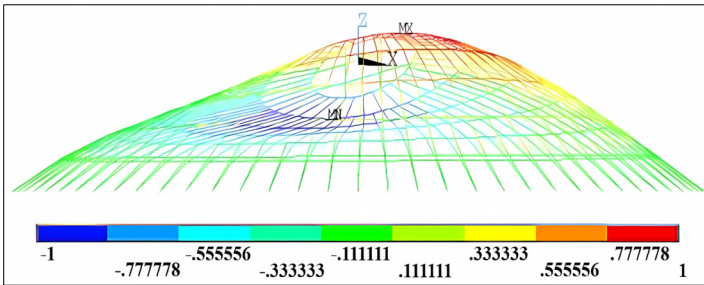


Fig. 11. Second order buckling mode

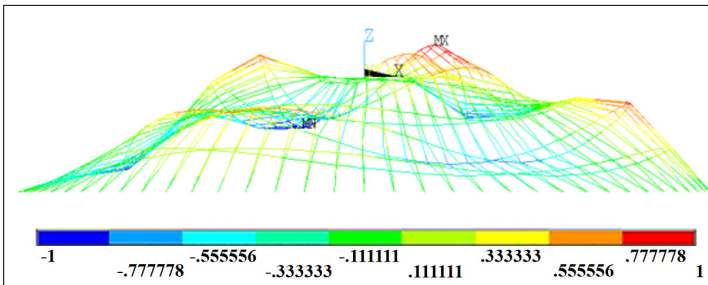


Fig. 12. Third order buckling mode

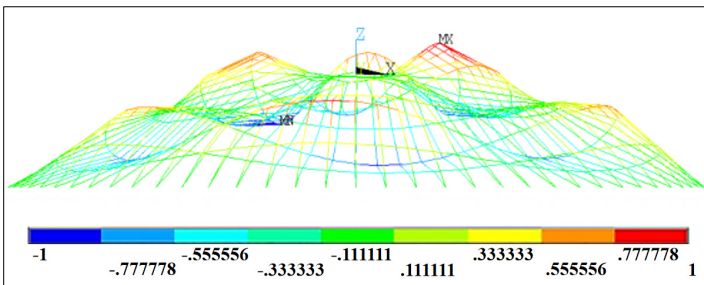


Fig. 13. Fourth order buckling mode

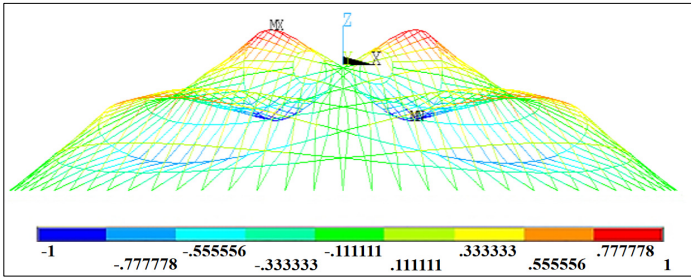


Fig. 14. Fifth order buckling mode

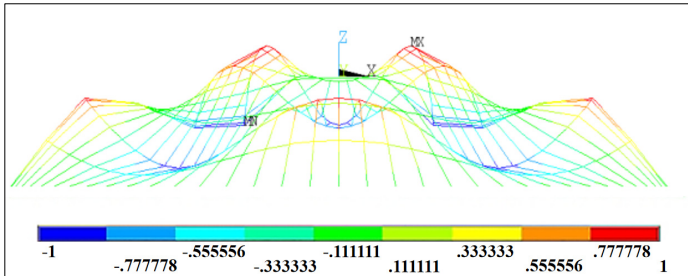


Fig. 15. Sixth order buckling mode

4.2 Effect of Initial Geometric Defects on Nonlinear Stability of LNG Mesh Shell Structures

JGJ7-2010 stipulates that the effect of initial geometric defects on the structure needs to be considered when analyzing the whole process of single-layer mesh shell structure. In this paper, the size of initial geometric defects is set to be 1/300, 1/500, 1/700 and 1/1000 of the structural span for comparison. The nonlinear stability analysis is carried out for the tank mesh shell structure considering double nonlinearity, and the full span live load of 750 Pa is applied to the mesh shell structure, and the analysis results are shown in Fig. 16 and Table 7.

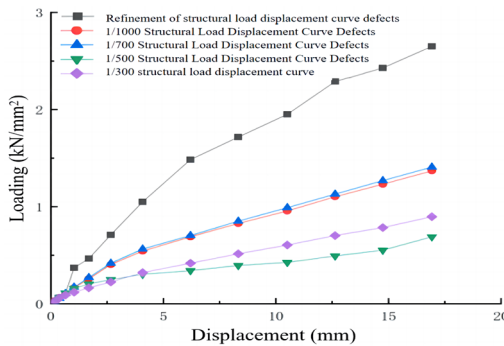


Fig. 16. Load-displacement curves of different geometric defects

Table 7. Stress results of reticulated shell under three working conditions

Defect mplitude Model	Flawless	1/1000	1/700	1/500	1/300
Overall model	2.97	2.35	2.05	2.02	1.85

Taking the overall structural model as an example, the ultimate load carrying capacity in the case of only considering the material nonlinearity is 2.97kN/m^2 , which is 46% lower than the linear elastic first-order buckling load of 5.45kN/m^2 . Considering the amplitude of the double nonlinear defects as 1/300 as an example, the ultimate load carrying capacity is 1.85kN/m^2 , which is 66% lower than that in the case of linear elastic buckling load and 38% lower than that in the case of only considering the material nonlinearity. The double nonlinear stability determines the value of the minimum load carrying capacity of this LNG tank mesh shell structure, and a double nonlinear stability analysis should be performed when designing the mesh shell.

The existence of initial geometric defects makes the model ultimate load carrying capacity are reduced, with the initial geometric defect amplitude increases, the mesh shell ultimate load carrying capacity also has a significant decrease, the initial geometric defect amplitude in 1/700 below, the four kinds of ultimate load carrying capacity and the perfect structure is closer to the initial geometric defects, so the initial geometric defects are recommended to take the initial geometric defects in the mesh shell structure of the span of less than 1/700.

The load distribution and the way the mesh shell is connected to the substructure have a great influence on the stability of the mesh shell, which needs to be deeply explored and comprehensively considered.

5 Effects of Different Seismic Waves on the Dynamic Performance of LNG Mesh Shell Structures

The EL-centro wave x-direction, Taft wave x-direction and SHM2 seismic wave are selected to analyze the seismic time course of the LNG dome mesh shell structure, and the peak values of the three seismic waves are adjusted to 400 gal. The maximum nodes of the mesh shell structure displaced by the above three seismic waves are at node 175, node 202, and node 270, respectively. The displacement time-range curves of the nodes in different directions are shown in Figs. 17-25.

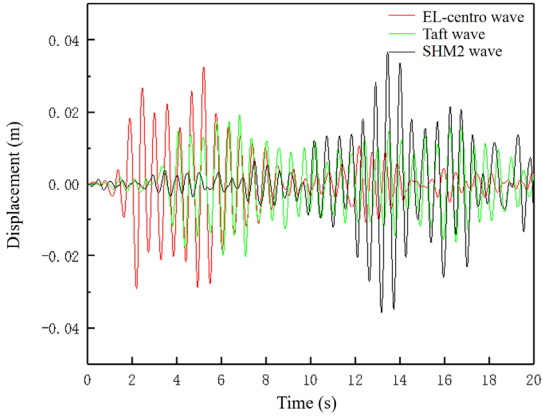


Fig. 17. Node 175 X-direction displacement

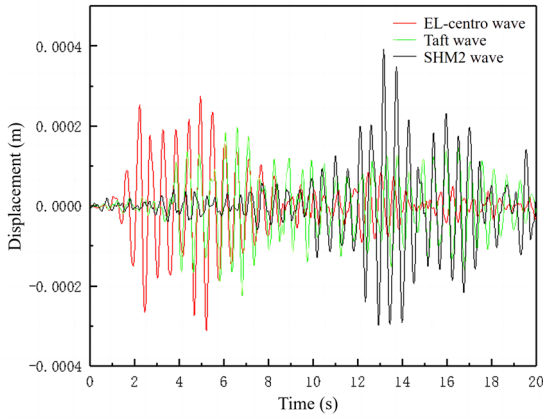


Fig. 18. Node 175 Y-direction displacement

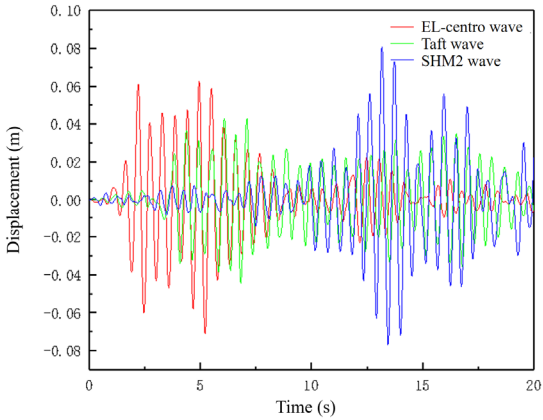


Fig. 19. Node 175 Z-direction displacement

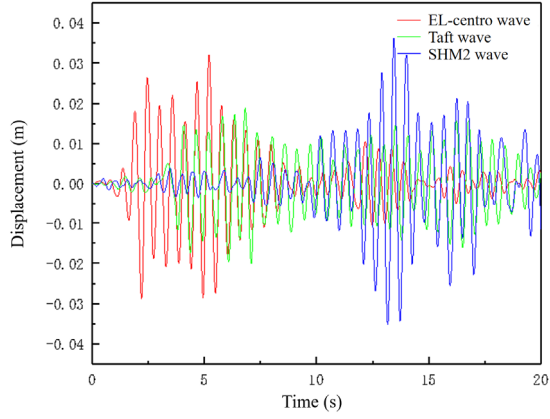


Fig. 20. Node 202 X-direction displacement

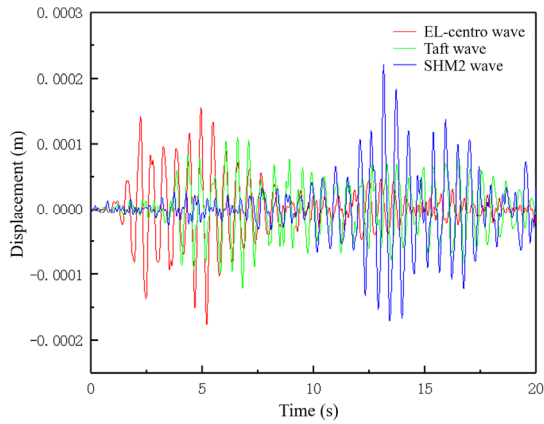


Fig. 21. Node 202 Y-direction displacement

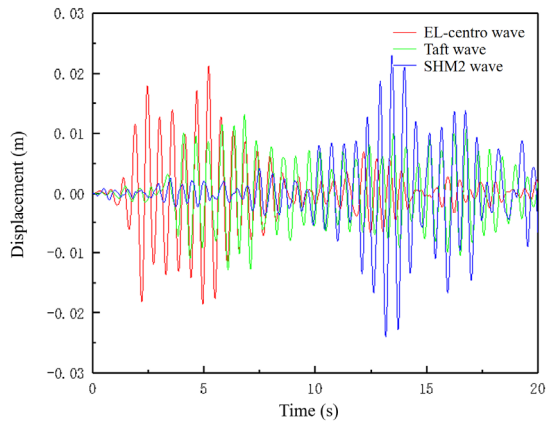


Fig. 22. Node 202 Z-direction displacement

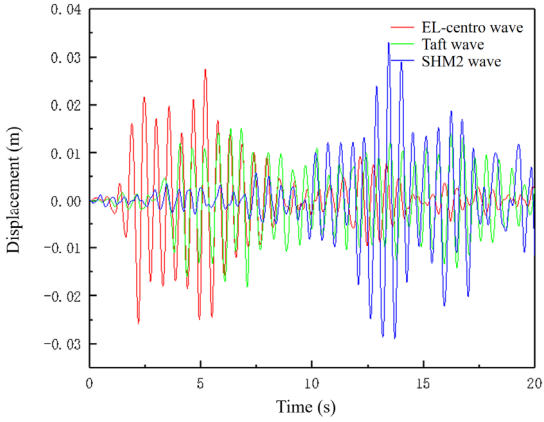


Fig. 23. Node 270 X-direction displacement

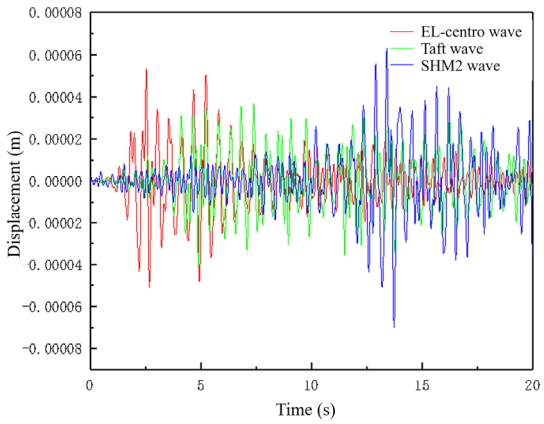


Fig. 24. Node 270 Y-direction displacement

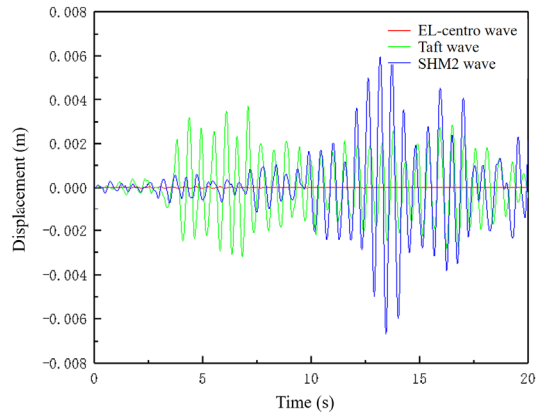


Fig. 25. Node 270 Z-direction displacement

The displacements of the three selected nodes are very different, and overall the displacements in the x- and z-directions of the three nodes are much larger than the y-direction displacements. Taking the EL-centro wave as an example, the maximum displacement of the structure in the x-direction at node 175 is 3.2 mm, the maximum displacement in the z-direction is 6.2 mm, and the maximum displacement in the y-direction is 0.027 mm. It can be inferred that the seismic response of the whole structure is larger in the x-direction and z-direction, while the response in the y-direction is smaller.

The axial force distribution of the mesh-shell structure at the end of different seismic actions is shown in Figs. 26-28.

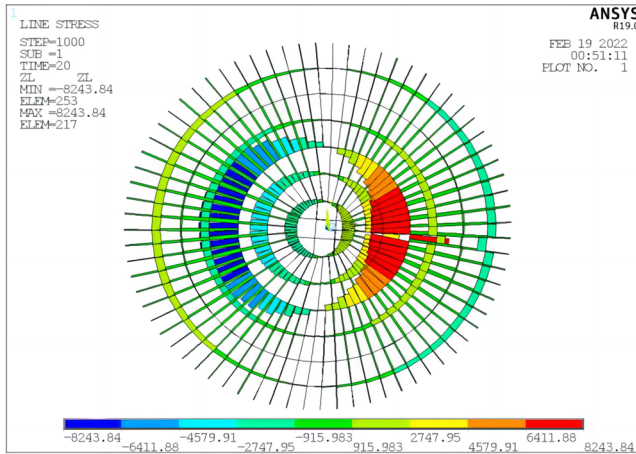


Fig. 26. EL-centro wave axial force distribution map

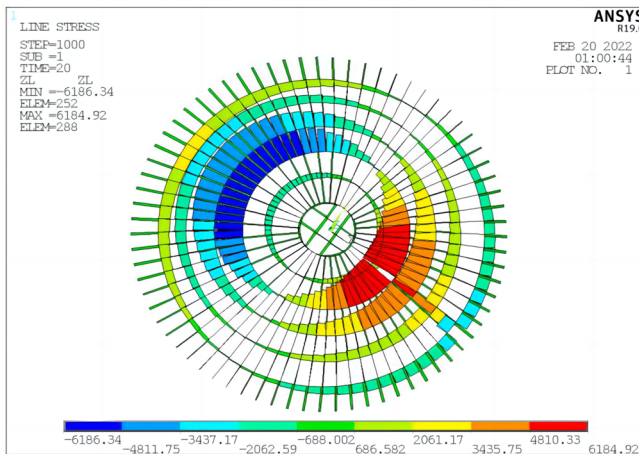


Fig. 27. Taft wave axial force distribution map

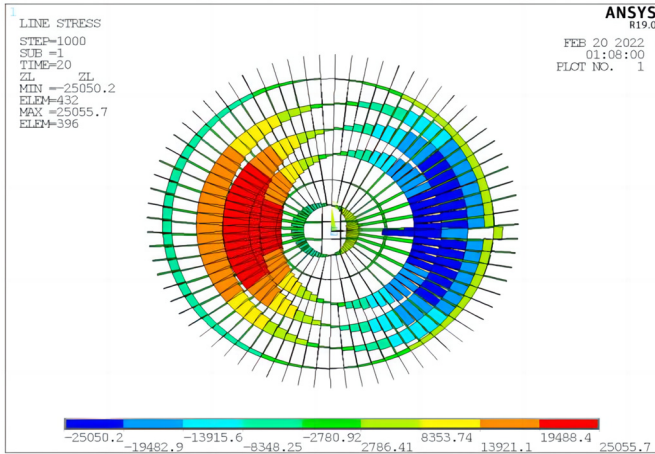


Fig. 28. SHM2 wave axial force distribution map

The maximum axial force of the mesh-shell structure occurs in the vicinity of the third ring and the maximum axial force diagram shows a symmetrical distribution under the action of three kinds of seismic waves. Therefore, in order to ensure the durability and safety of the structure, the structural design should be strengthened from the second ring to the fourth ring.

6 Conclusions

The displacement of LNG dome mesh shell structure under three working conditions is much less than 122mm, and the maximum stress value of the structure is less than the permissible stress value of Q345 material, which is in line with the requirements of the mesh shell structure in terms of stiffness and strength, and it has a better bearing capacity and stability performance.

(2) The flexural modal deformation of the mesh shell shows symmetric deformation, due to the symmetric distribution of the mass and stiffness of the single-layer mesh shell structure, the first 20 orders of the eigenvalue of the flexural coefficient of the adjacent two orders of the value of the change is not large, indicating that the structure is reasonably designed, and good performance of the force.

(3) The single-layer mesh shell structure is a defect-sensitive structure, the initial geometric defects will significantly reduce the ultimate load carrying capacity of the structure; the ultimate load carrying capacity of the structure decreases with the increase of the magnitude of the defects, and when the magnitude of the initial geometric defects is less than 1/700, there is no significant difference between the ultimate load carrying capacity and the perfect structure, so it is recommended that the initial geometric defects take a value lower than the 1/700 of the span of the mesh shell structure.

(4) Different seismic waves have a great influence on the shape of the displacement time curve of the structure. Under different one-dimensional seismic effects in the X direction, the displacement of the structure along the X-axis and Z-axis is larger, and

the maximum value of the axial force of the rods occurs in the vicinity of the third ring of the mesh-shell structure, which needs to be reinforced locally.

Acknowledgment

Natural Science Foundation of Heilongjiang Province of China (LH2020E018)

References

1. Chen Z .Structure Design and Stability Calculation of Large Storage Tanks with a Reticulated Shell Dome[J].Journal of Mechanical Engineering, 2015, 51(6):36-44.
2. Cheng X , Wu Z , Zhen C ,et al.A novel stability analysis method of single-layer ribbed reticulated shells with roof plates[J].Thin-Walled Structures, 2024, 200.
3. Karman, Von T. The Buckling of Spherical Shells by External Pressure[J]. Journal of the Aeronautical Sciences, 1939, 7(2):43-50.
4. Fan F, Cao Z, Shen S. Elasto-plastic stability of single-layer reticulated shells[J]. Thin-Walled Structures, 2010, 48(10-11): 827-836.
5. Mashrah W A H, Rima B, Liu H, et al. Static stability analysis of steel single-layer spherical latticed shells with and without roofing systems[J]. Journal of Building Engineering, 2023, 77: 107141.
6. Yu P, Yun W, Bordas S, et al. Static stability analysis of single-layer reticulated spherical shell with kiewitt-sunflower type[J]. International Journal of Steel Structures, 2021, 21: 1859-1877.
7. YE Jihong, SHEN Zuyan. Experimental study of dynamic stabilization of single-layer mesh-shell structures[J]. Space Structure, 1997, 3(2):7. DOI:CNKI:SUN:KJJG.0.1997-02-004.

Open Access This chapter is licensed under the terms of the Creative Commons Attribution-NonCommercial 4.0 International License (<http://creativecommons.org/licenses/by-nc/4.0/>), which permits any noncommercial use, sharing, adaptation, distribution and reproduction in any medium or format, as long as you give appropriate credit to the original author(s) and the source, provide a link to the Creative Commons license and indicate if changes were made.

The images or other third party material in this chapter are included in the chapter's Creative Commons license, unless indicated otherwise in a credit line to the material. If material is not included in the chapter's Creative Commons license and your intended use is not permitted by statutory regulation or exceeds the permitted use, you will need to obtain permission directly from the copyright holder.

